PCCP

PAPER

View Article Online
View Journal | View Issue

Cite this: *Phys. Chem. Chem. Phys.*, 2015, **17**, 19039

The electronic structure of quasi-free-standing germanene on monolayer MX (M = Ga, In; X = S, Se, Te)†

Zeyuan Ni, Emi Minamitani, Yasunobu Ando and Satoshi Watanabe*

Received 27th April 2015,
Accepted 22nd June 2015

DOI: 10.1039/c5cp02428e

www.rsc.org/pccp

For the first time by using the *ab initio* density functional theory, the stability and electronic structures of germanene on monolayer GaS, GaSe, GaTe and InSe have been investigated. Germanene preserves its buckled-honeycomb structure on all the studied substrates similar to the free-standing case. Moreover, germanene stays neutral and preserves its Dirac-cone-like band structure on monolayer GaTe and InSe. In these two cases, a bandgap of 0.14–0.16 eV opens at the Dirac point of germanene, while the effective masses remain as small as 0.05–0.06 times the free-electron mass. The estimated carrier mobility is up to 2.2 × 10^5 cm^2 V^{-1} s^{-1}. These features show that monolayer GaTe and InSe are promising as substrates for germanene devices.

Introduction

Graphene, the first 2-dimentional (2D) material, is known for its ultrahigh carrier mobility up to 2 × 10^5 cm^2 V^{-1} s^{-1} in suspended samples[1] and 4 × 10^4 cm^2 V^{-1} s^{-1} on a SiO_2 substrate,[2] which makes it attractive for application in electronic devices. Unfortunately, it remains challenging to open a band gap in graphene and preserve its extreme carrier mobility at the same time. Such a dilemma stimulates the search for other 2D materials, for example silicene and germanene, the Si and Ge cousins of graphene.[3,4] Silicene and germanene have been successfully synthesized recently on several substrates (*e.g.* Ag(111),[5–9] Ir(111)[10] and ZrB_2[11,12] for silicene; Pt(111),[13] Au(111)[14] and Al(111)[15] for germanene) in experiments, and the first silicene field-effect transistor (FET) has been fabricated.[16] Free-standing silicene and germanene are predicted to be new members of Dirac materials and share most of the amazing properties of graphene, *e.g.* the ultrahigh carrier mobility and the quantum spin Hall effect (QSHE).[17] Additionally, due to their unique buckled structure, monolayer (ML) silicene and germanene show many behaviors different from those of the ML graphene, such as the tunable bandgap by electric-field[18,19] or surface atom adsorption,[20,21] and much stronger spin–orbit interaction,[22,23] displaying great potential in electronic and spintronic applications. Among the three mentioned materials, germanene is predicted to have the highest intrinsic carrier mobility in theory, which is about twice as high as that of graphene.[24] Germanene is also predicted to have the strongest spin–orbit (SO) interaction among the three with a SO gap over 23 meV,[22,23] which makes the high-temperature QSHE possible,[22] while the SO gap of silicene and graphene is only 1.55 meV[22] and 8 μeV,[25] respectively.

However, germanene shares a problem with silicene: one cannot utilize germanene's ultimate properties unless suitable substrates are found for germanene. Currently, ML germanene can only be synthesized on metal surfaces, such as Au(111)[14] and Pt(111),[13] but electronic devices such as FETs require substrates with a large band gap. Moreover, many semiconducting substrates such as bare SiO_2 and GaAs will strongly interact with germanene and destroy its Dirac cone.[18,26] Although germanene is reported to have weak interaction with the fully hydrogenated GaAs (0001) surface,[26] it is hard in practice to prepare an atomically flat and perfectly hydrogenated GaAs surface – the existence of defects may still ruin germanene. In addition, free-standing germanene changes from Dirac material to normal metal when the tensile or compressive strain reaches 5%,[27,28] indicating the sensitivity of germanene to structural deformation. From the above, we can say that germanene still lacks an appropriate substrate to serve as a promising electronic material.

On the other hand, ML group III monochalcogenides MX (M = Ga, In; X = S, Se, Te), a new family of 2D materials, are predicted to have a large bandgap of 2–3 eV.[29] Recently, ML and few-layer GaS,[30,31] GaSe[30,32] and InSe[33] with an atomically flat surface have been successfully fabricated in experiment. Some of the MX like GaS and GaSe are predicted to have weak interaction with silicene in theory.[34,35] Although MX seem promising as the suitable substrates for germanene, the interaction between them and germanene is yet to be investigated.

Department of Materials Engineering, The University of Tokyo, Tokyo 113-8656, Japan. E-mail: zeyuan_ni@cello.t.u-tokyo.ac.jp, watanabe@cello.t.u-tokyo.ac.jp

† Electronic supplementary information (ESI) available. See DOI: 10.1039/c5cp02428e

In this article, we study the structural and electronic behaviors of ML germanene on ML GaS, GaSe, GaTe and InSe for the first time by using the density functional theory (DFT). The Dirac-cone-like band structure of germanene on these substrates is preserved. Germanene is found to be semiconducting on GaTe and InSe with a band gap above 0.1 eV, while its effective masses at the Dirac point remain as small as 0.05–0.06 m_0 (free electron mass), leading to an ultrahigh carrier mobility estimated to be around 1.5–2.2 $\times$ 10^5 cm^2 V^{-1} s^{-1}.

We use the DFT method implemented in Quantum ESPRESSO[36] to perform geometry optimization and electronic structure calculation and VASP[37] to perform hybrid functional calculation. In Quantum ESPRESSO calculation, ultrasoft pseudopotentials with nonlinear core correction are employed. The optB86b-vdw[38–41] exchange–correlation functional is used in geometry optimization to take the van der Waals interaction into account. The generalized gradient approximation (GGA) exchange–correlation functional of the Perdew, Burke, and Ernzerhof (PBE) parametrization[42] is used in electronic structure calculation with spin–orbital coupling (SOC). After the convergence test, the wave function cutoffs are chosen to be 952, 952, 1360, 816 eV for GaS, GaSe, GaTe and InSe, respectively, and the charge density cutoffs are chosen to be 10 times of them. A Monkhorst–Pack[43] (MP) k-point grid of 21 $\times$ 21 $\times$ 1 is chosen. The dipole correction[44] is engaged and found to have a negligible influence in our system. In VASP calculation, the projected augmented wave (PAW)[45] pseudopotential is employed. The Heyd–Scuseria–Ernzerhof (HSE06) functional[46–48] is used in hybrid functional calculation without SOC due to computational overburden. The corresponding MP k-point and q-point grids are both 27 $\times$ 27 $\times$ 1.

The initial structures of free standing ML MX (GaS, GaSe, GaTe and InSe) and germanene are adopted from previous literature[17,29] (Fig. 1(a) and (b)). They have similar honeycomb structures and lattice constants of 3.58–4.06 Å, not far from that of germanene (4.02 Å), so only the 1 $\times$ 1 stacking (Fig. 1e) is considered in this work. There are three high symmetric points in one hexagonal cell and two different atoms in germanene after stacking, so there are $\binom{3}{2} = 6$ high symmetric stacking configurations in total (Fig. 1(c)). The six configurations are characterized by their stacking mode (AA or AB) and the type of the Ge atom (top "t" or bottom "b") which overlaps the substrate atom (metal M or chalcogen X) in the top view: AA-t (AA-X-t or AA-M-b), AA-b (AA-X-b or AA-M-t), AB-M-t, AB-M-b, AB-X-t, and AB-X-b.

We begin from the investigation of the most energetically favorable configurations of germanene on ML MX. First, the lattice constant is determined. We choose one stacking configuration (AA-t) to obtain the most preferable lattice constant and apply it to the other configurations. The optimized lattice constant is shown in Table 1. GaS and GaSe have smaller lattice constant with germanene than in their free standing or bulk case, while GaTe and InSe are almost unchanged. This is probably due to the fact that the free standing germanene is predicted to have a lattice constant of 3.97–4.03 Å,[17,24] larger than those of GaS and GaSe and close to those of GaTe and InSe. The lattice constant of germanene on GaTe with AB-M-b configuration is also examined and the result is similar to the above. Second, we fix the lattice constant and optimize the geometry using all the six configurations as the initial ones. The configuration with the lowest energy is found to be the same for all the four MX, which is shown in Fig. 1(d) and (e) and is named as the AB-M-b configuration (AB stacking, M atom above b-Ge). The total energy differences between the most favorable configuration and the others, which are presented in Fig. 1(f), are about 0.1 eV except for

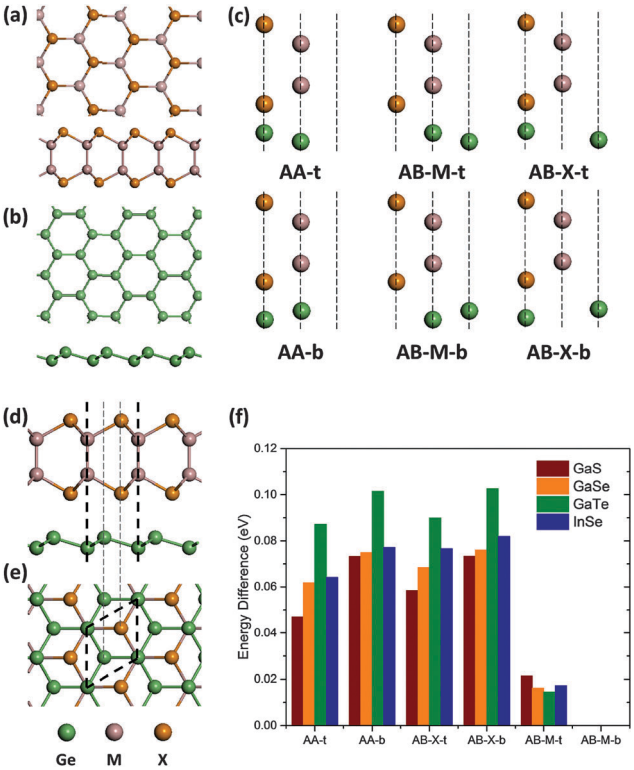

Fig. 1 Top and side views of free standing ML (a) MX and (b) germanene. (c) All the six high symmetric stacking configurations of germanene on MX. (d) Side and (e) top views of 1 $\times$ 1 stacked ML germanene and MX with the most preferable stacking. Thick dashed lines denote the lattice, and thin dashed lines denote the high symmetric positions in hexagonal cells. M = Ga, In; X = S, Se, Te. (f) Energy difference between AB-M-b configuration and the other configurations.

Table 1 Structural parameters of bulk MX in experiments, ML MX in theory from previous literature (ref. 29), and germanene on ML MX in this work. Experimental data are provided by the Inorganic Crystal Structure Database (ICSD)[60]

	MX only		Germanene–MX		
	Lattice (Å)		Lattice (Å)	z-Distance (Å)	Germanene buckling (Å)
	Bulk	ML DFT	ML		
	Experiment	(HSE)	This work		
GaS	3.59	3.58	3.78	2.90	0.89
GaSe	3.74–3.76	3.75	3.89	2.99	0.77
GaTe	4.06	4.06	4.06	3.05	0.71
InSe	4.00–4.05	4.02	4.03	2.92	0.71

the AB-M-t configuration. Although the energy difference between AB-M-b and AB-M-t configurations is only ~0.02 eV, they cannot be easily transformed into each other. This is because they are not related by any in-plane translation but a space inversion of the germanene part, and the transformation energy barrier between them is about 0.3 eV (Fig. S1, ESI†). Other non-high-symmetric configurations are also considered for germanene on GaTe and are found to be less favorable (Fig. S3, ESI†). Hence, we focus on the AB-M-b stacking of germanene on all kinds of ML MX in the following. The vertical distance between MX and germanene is 2.90–3.05 Å, and the nearest distance between the Ge atom and the X atom is about 3.63–3.85 Å. Such a far distance suggests the weak interaction between germanene and MX substrates. The buckling of germanene is enhanced from the free-standing value of 0.64–0.69 Å[17,18,24] to 0.77–0.89 Å on GaS and GaSe, which can be understood easily from the smaller lattice constant than in the free-standing case. However, the buckling of germanene is still slightly enhanced to 0.71 Å on GaTe and InSe, where the lattice constants are larger than that of the free-standing germanene. This implies that the interaction is non-negligible.

Next we investigate whether germanene also has a well-preserved electronic structure. The charge transfer from germanene to MX estimated using the Bader charge analysis[49–51] with the PBE functional is as small as 0.02 (GaTe and GaSe), 0.03 (InSe) and 0.04 (GaS) electrons. The charge transfer estimated with the HSE functional give similar results (Table 2). Since the total dipole is mainly induced by the charge transfer, the strength of the dipole correction in the Hartree potential is in the same sequence as above, specifically 0.03 (GaTe) < 0.08 (GaSe) < 0.14 (InSe) < 0.23 (GaS) eV Å^{-1} (Table 2 and Fig. S4, ESI†). The differential charge densities $\rho_{\mathrm{diff}} = \rho_{\mathrm{germanene-MX}} - \rho_{\mathrm{germanene}} - \rho_{\mathrm{MX}}$ (shown in Fig. S5, ESI†) reveal that the charge density in the interspace between germanene and MX increases, while the density near both Ge and X atoms decreases.

The band structures of germanene on ML MX are presented in Fig. 2. All of the four compound systems have Dirac-cone-like band structures at the *K*-point with a "gap" opened (named as the Dirac-gap to prevent confusion with the band gap). Such a Dirac-gap can be attributed to germanene according to the projected band structure shown in the left panel of Fig. 2, which shows the Ge contribution is over 89% at the Dirac point of germanene and rules out the possibility that these states mainly come from the MX substrates. The Dirac-gap appears in germanene on all kinds of MX, but only germanene on GaTe and InSe is actually semiconducting. Germanene on GaS and GaSe is metallic due to the bands crossing the Fermi level near the Γ-point. This metallic behavior is caused by the cooperation of the deformation of germanene and the interaction with the MX substrate. Germanene on GaS and GaSe in a 1×1 cell has a compressive strain of 6% and 3%, respectively. As mentioned previously, germanene changes from Dirac material to metal at a compressive strain beyond 5% due to the band lifting at the Γ-point ("self-induced doping"), though no Dirac-gap opens.[27] The band structures of the germanene-part of the germanene–GaS and –GaSe systems have similar band lifting at the Γ-point (Fig. S6, ESI†). It is worth mentioning that germanene on GaTe and InSe also has a little band lifting at the Γ-point in spite of the fact that the strain is no larger than 1% (Fig. S6, ESI†), which can only be explained by the interaction between germanene and MX.

Table 2 Charge transfer from germanene to MX in number of electrons, and the Dirac-gap, SOC-split and effective masses at the Dirac point of germanene on MX. Note that although germanene has a gap at the Dirac point on GaS and GaSe, it is still metal due to the band lifting near the Γ point crossing the Fermi level, so their gap sizes and effective masses have no practical meaning except for comparison

		GaS	GaSe	GaTe	InSe
Charge transfer (e)	PBE	0.04	0.02	0.02	0.03
	HSE	0.03	0.03	0.02	0.04
Dipole correction (eV Å^{-1})	PBE	0.23	0.08	0.03	0.14
Dirac-gap (eV)	PBE	0.14	0.13	0.12	0.11
	PBE + SOC	0.11	0.10	0.10	0.08
	HSE	0.18	0.16	0.16	0.14
SOC-split (eV)	Conduction band	0.030	0.024	0.015	0.021
	Valence band	0.034	0.028	0.024	0.042
$m^*_{\Gamma K}$ (m_0)	$m^*_{\mathrm{e\_h}}$	0.089	0.078	0.081	0.080
	$m^*_{\mathrm{e\_l}}$	0.061	0.056	0.062	0.050
	$m^*_{\mathrm{h\_l}}$	0.060	0.055	0.059	0.049
	$m^*_{\mathrm{h\_h}}$	0.088	0.076	0.076	0.076
$m_{KM}{}^*$ (m_0)	$m^*_{\mathrm{e\_h}}$	0.087	0.078	0.078	0.078
	$m^*_{\mathrm{e\_l}}$	0.057	0.051	0.058	0.044
	$m^*_{\mathrm{h\_l}}$	0.056	0.051	0.054	0.043
	$m^*_{\mathrm{h\_h}}$	0.088	0.075	0.073	0.074

The size of the Dirac-gaps in germanene on different MX are summarized in Table 2. In general, the Dirac-gap of germanene on MX decreases in the order of GaS > GaSe > GaTe > InSe from 0.14 to 0.11 eV when estimated using the PBE functional without SOC. The opening of the Dirac-gap can be attributed to the breaking of the inversion symmetry by introducing the MX substrate, similar to the band gap opening in germanene by the vertical electric field.[18] If the SOC is considered in calculations with the PBE functional, the conduction and valence bands split into two bands by 0.02–0.04 eV (Table 2, Fig. 2 and 3), respectively, involving the Dirac-gap decrease by 0.02–0.03 eV. Moreover, it is well known that DFT can underestimate the actual band gap of semiconductors by up to 50%. The use of the hybrid functional, which includes a certain amount of the Hartree–Fock exchange, can yield much improved band gap values compared with the GGA functionals.[46] As shown in Table 2, the Dirac-gap given by the HSE hybrid functional is about 0.16–0.18 eV, ~25% larger than the PBE cases. The actual band gap of germanene on MX should be a little smaller than the HSE band gap due to the SOC splitting. Regretfully, the HSE calculation including SOC is not feasible within our available computational resources. Assuming that the SOC splitting is the same as the PBE calculation results, we estimate the actual Dirac gap to be around 0.1 eV. In the cases of germanene on GaTe and InSe, the 0.1 eV Dirac-gap also corresponds to the band gap. If combined with other band-gap-opening techniques, such as the application of vertical electric field[18] and the surface atom adsorption,[21] the band gap in these cases could possibly

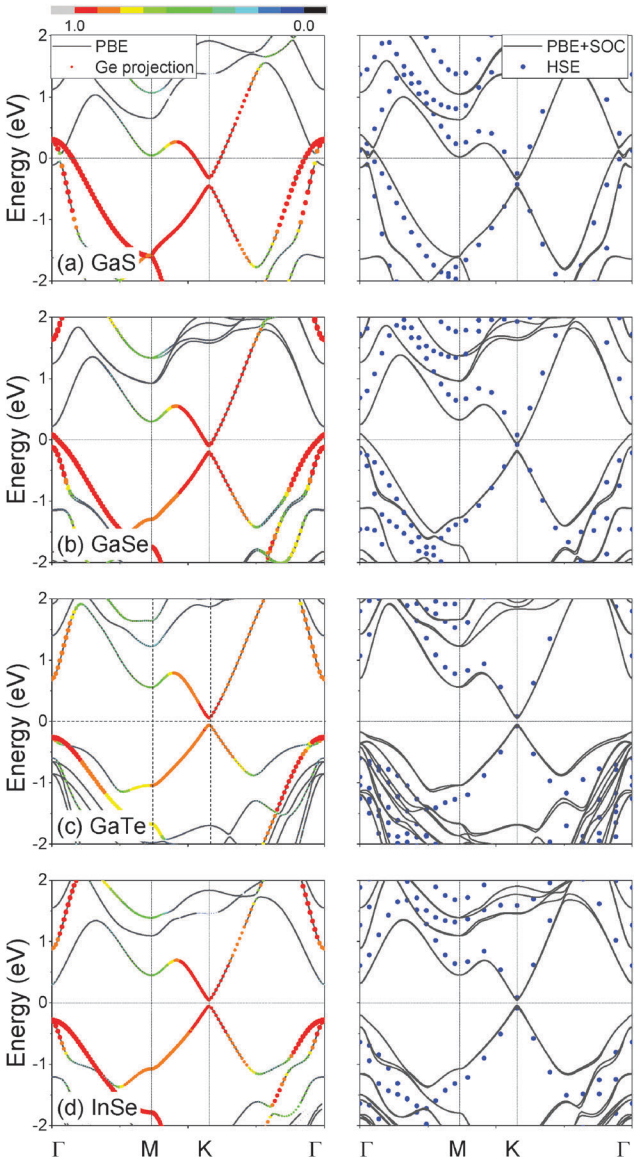

Fig. 2 Band structures of germanene on (a) GaS, (b) GaSe, (c) GaTe and (d) InSe. The left panel is the band structures obtained using the PBE functional (black lines) and the Ge projections (size indicates the absolute projection value, and color indicates the percentage of Ge contribution in total with red standing for 90–100%), and the right panel is the band structures obtained using the PBE + SOC (black lines) and HSE without SOC (blue dots).

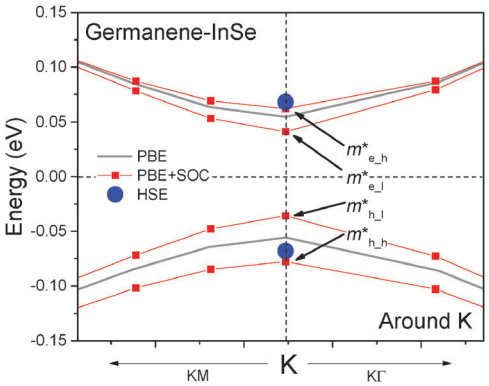

Fig. 3 Details of the band structure of germanene on InSe near the Fermi level (dashed horizontal line) and *K* point.

reach 0.4 eV, which is the minimum requirement as the channel material of field effect transistors.[52] Note that contrary to the result given by the PBE functional, germanene on GaSe is predicted to be also semiconducting by the HSE calculation with a band gap of 0.16 eV. The reason is that the valence band at the Γ point is lowered to about 0.2 eV below the Fermi level in the HSE calculation, while the same band in the PBE calculation is above the Fermi level. Such a phenomenon of the lowered valence band at the Γ point in HSE calculations can also be found in other MX substrates (right panel of Fig. 2). Note that we have confirmed the reliability of our calculations by examining the HSE band structure of the free-standing germanene (Fig. S7, ESI†): it agrees well with the previous literature.[53] We have also tried the GW calculation, but found it computationally too heavy within our available computational resources.

Although a band gap opens, germanene still has ultrahigh carrier mobility on GaTe and InSe as shown below. The SOC splitting introduces extra effective masses compared to non-SOC cases, namely the heavy hole/electron masses $m^*_{h\_h}/m^*_{e\_h}$ and light hole/electron masses $m^*_{h\_l}/m^*_{e\_l}$ along the *KM* and *KΓ* directions (Fig. 3). The effective masses calculated by quadratic polynomial fitting of the band structure are listed in Table 2. The light m^* along *KM* remains as small as $\sim 0.05\ m_0$, where m_0 is the free electron mass, on GaTe and $\sim 0.04\ m_0$ on InSe, and the heavy m^* are just about 0.01 m_0 higher. The m^* along *KΓ* is only 0.004–0.006 m_0 larger than the corresponding m^* along *KM*, so they can be treated as almost the same. The relaxation time τ of free-standing germanene at room temperature, estimated using the deformation potential method including the electron-acoustic phonon scattering mechanism,[24] is 5.3 ps. Considering the fact that graphene and graphite have similar phonon dispersion[54,55] and relaxation time[24,56] and that germanene and MX are connected through van der Waals interaction as in the case of graphite, it would be acceptable in the first rough estimation of the mobility to assume that germanene has similar τ on MX to that of the free-standing case. Given τ is the same as the free-standing case, the mobility in germanene calculated by $\mu = e\tau/m^*$ can be up to 1.5 and 2.2×10^5 cm^2 V^{-1} s^{-1} for light carriers, and still above 1.2×10^5 cm^2 V^{-1} s^{-1} for heavy carriers. The light carrier mobility is close to the best value of graphene obtained in suspended samples in experiment, around 2×10^5 cm^2 V^{-1} s^{-1} [1], and the intrinsic carrier mobility of free-standing graphene ($3.2–3.5 \times 10^5$ cm^2 V^{-1} s^{-1}) and silicene ($2.2–2.6 \times 10^5$ cm^2 V^{-1} s^{-1}) in theory.[24] If graphene is put on a substrate like SiO_2, its carrier mobility will drop to 10^4 cm^2 V^{-1} s^{-1} or lower.[2] In addition, the high mobility in graphene and silicene will degrade significantly if a band gap of over 0.1 eV is opened.[57,58]

Admittedly, the relaxation time of germanene could be affected by the existence of a MX substrate, so the above estimation of carrier mobility might be just an estimation for the order of magnitude. More elaborated estimation of carrier mobility is left as a future problem. In doing so, methods like

the deformation potential model[24,59] can be used to examine the relaxation time of MX-supported germanene. Note that optical phonon may have to be taken into account in addition to the acoustic phonon. We say so because our preliminary molecular dynamics (MD) simulation shown in the ESI† indicates that the magnitude of ZO phonon is large at high temperature (Fig. S8, ESI†). On the other hand, we would like to note that our MD simulation has been performed just to see whether germanene can preserve its hexagonal lattice well on GaTe at 500 K, and strong phonon modes do not necessarily have strong electron–phonon coupling.

It should also be noted that in experiment, the ML MX itself will need a substrate. However, it does not affect our conclusions due to the following two reasons. First, the lattice constant of ML MX can be preserved on some common substrates like SiO_2. For example, atomic layers of InSe on SiO_2 have a lattice constant of 0.40 nm,[33] similar to the free-standing case and our result. Hence, the advantage of small lattice mismatch between germanene and InSe will be preserved even if InSe is put on SiO_2. Second, germanene can also retain its Dirac cone on thicker few-layer MX, and the thickness can screen out the effect of the substrate under MX. According to our calculation, germanenes on ML and trilayer InSe have similar band structures (Fig. S10, ESI†), probably because InSe layers are stacked with the weak van der Waals interaction. Using the bulk MX itself as the substrate is probably another good choice. If a clean and flat (001) surface of the bulk MX is made with little defects, it may also serve as a suitable substrate for germanene.

In conclusion, for the first time by using the density function theory, we predict that germanene can preserve its low-buckled honeycomb structure and the Dirac-cone-like band structure similar to the free-standing case. Furthermore, germanene is predicted to be semiconducting on GaTe and InSe with a band gap of over 0.1 eV, while an ultrahigh carrier mobility estimated up to 2.2×10^5 cm^2 V^{-1} s^{-1} is preserved. The band splitting caused by the SOC can be up to 42 meV. Hence, we believe germanene on GaTe and InSe has potential in electronic and spintronic applications. Our research would stimulate the synthesis of high-performance germanene and its FET in the future.

Acknowledgements

This work has been supported by a Grant-in-Aid for Scientific Research on Innovative Areas No. 26107514 from MEXT, Japan.

References

1 K. I. Bolotin, K. J. Sikes, Z. Jiang, M. Klima, G. Fudenberg, J. Hone, P. Kim and H. L. Stormer, *Solid State Commun.*, 2008, **146**, 351–355.
2 J.-H. Chen, C. Jang, S. Xiao, M. Ishigami and M. S. Fuhrer, *Nat. Nanotechnol.*, 2008, **3**, 206–209.
3 M. Xu, T. Liang, M. Shi and H. Chen, *Chem. Rev.*, 2013, **113**, 3766–3798.
4 P. Miró, M. Audiffred and T. Heine, *Chem. Soc. Rev.*, 2014, **43**, 6537.
5 B. Feng, Z. Ding, S. Meng, Y. Yao, X. He, P. Cheng, L. Chen and K. Wu, *Nano Lett.*, 2012, **12**, 3507–3511.
6 P. Vogt, P. De Padova, C. Quaresima, J. Avila, E. Frantzeskakis, M. C. Asensio, A. Resta, B. Ealet and G. Le Lay, *Phys. Rev. Lett.*, 2012, **108**, 155501.
7 A. Resta, T. Leoni, C. Barth, A. Ranguis, C. Becker, T. Bruhn, P. Vogt and G. Le Lay, *Sci. Rep.*, 2013, **3**, 2399.
8 C. L. Lin, R. Arafune, K. Kawahara, M. Kanno, N. Tsukahara, E. Minamitani, Y. Kim, M. Kawai and N. Takagi, *Phys. Rev. Lett.*, 2013, **110**, 076801.
9 C. L. Lin, R. Arafune, K. Kawahara, N. Tsukahara, E. Minamitani, Y. Kim, N. Takagi and M. Kawai, *Appl. Phys. Express*, 2012, **5**, 045802.
10 L. Meng, Y. Wang, L. Zhang, S. Du, R. Wu, L. Li, Y. Zhang, G. Li, H. Zhou, W. A. Hofer and H. J. Gao, *Nano Lett.*, 2013, **13**, 685–690.
11 A. Fleurence, R. Friedlein, T. Ozaki, H. Kawai, Y. Wang and Y. Yamada-Takamura, *Phys. Rev. Lett.*, 2012, **108**, 245501.
12 A. Fleurence, Y. Yoshida, C. C. Lee, T. Ozaki, Y. Yamada-Takamura and Y. Hasegawa, *Appl. Phys. Lett.*, 2014, **104**, 021605.
13 L. Li, S. Z. Lu, J. Pan, Z. Qin, Y. Wang, Y. Wang, G. Cao, S. Du and H. Gao, *Adv. Mater.*, 2014, **26**, 4820–4824.
14 M. E. Dávila, L. Xian, S. Cahangirov, A. Rubio and G. Le Lay, *New J. Phys.*, 2014, **16**, 095002.
15 M. Derivaz, D. Dentel, R. Stephan, M.-C. Hanf, A. Mehdaoui, P. Sonnet and C. Pirri, *Nano Lett.*, 2015, **15**, 2510–2516.
16 L. Tao, E. Cinquanta, D. Chiappe, C. Grazianetti, M. Fanciulli, M. Dubey, A. Molle and D. Akinwande, *Nat. Nanotechnol.*, 2015, **10**, 227–231.
17 S. Cahangirov, M. Topsakal, E. Aktürk, H. Šahin and S. Ciraci, *Phys. Rev. Lett.*, 2009, **102**, 236804.
18 Z. Ni, Q. Liu, K. Tang, J. Zheng, J. Zhou, R. Qin, Z. Gao, D. Yu and J. Lu, *Nano Lett.*, 2012, **12**, 113–118.
19 N. D. Drummond, V. Zólyomi and V. I. Fal'Ko, *Phys. Rev. B: Condens. Matter Mater. Phys.*, 2012, **85**, 075423.
20 R. Quhe, R. Fei, Q. Liu, J. Zheng, H. Li, C. Xu, Z. Ni, Y. Wang, D. Yu, Z. Gao and J. Lu, *Sci. Rep.*, 2012, **2**, 853.
21 M. Ye, R. Quhe, J. Zheng, Z. Ni, Y. Wang, Y. Yuan, G. Tse, J. Shi, Z. Gao and J. Lu, *Phys. E*, 2014, **59**, 60–65.
22 C. C. Liu, W. Feng and Y. Yao, *Phys. Rev. Lett.*, 2011, **107**, 076802.
23 M. Ezawa, *Phys. Rev. Lett.*, 2012, **109**, 055502.
24 X.-S. Ye, Z.-G. Shao, H. Zhao, L. Yang and C.-L. Wang, *RSC Adv.*, 2014, **4**, 21216.
25 Y. Yao, F. Ye, X. L. Qi, S. C. Zhang and Z. Fang, *Phys. Rev. B: Condens. Matter Mater. Phys.*, 2007, **75**, 041401.
26 T. P. Kaloni and U. Schwingenschlögl, *J. Appl. Phys.*, 2013, **114**, 184307.
27 Y. Wang and Y. Ding, *Solid State Commun.*, 2013, **155**, 6–11.
28 T. P. Kaloni and U. Schwingenschlögl, *Chem. Phys. Lett.*, 2013, **583**, 137–140.
29 H. L. Zhuang and R. G. Hennig, *Chem. Mater.*, 2013, **25**, 3232–3238.

30 D. J. Late, B. Liu, H. S. S. R. Matte, C. N. R. Rao and V. P. Dravid, *Adv. Funct. Mater.*, 2012, **22**, 1894–1905.
31 P. Hu, L. Wang, M. Yoon, J. Zhang, W. Feng, X. Wang, Z. Wen, J. C. Idrobo, Y. Miyamoto, D. B. Geohegan and K. Xiao, *Nano Lett.*, 2013, **13**, 1649–1654.
32 S. Lei, L. Ge, Z. Liu, S. Najmaei, G. Shi, G. You, J. Lou, R. Vajtai and P. M. Ajayan, *Nano Lett.*, 2013, **13**, 2777–2781.
33 S. Lei, L. Ge, S. Najmaei, A. George, R. Kappera, J. Lou, M. Chhowalla, H. Yamaguchi, G. Gupta, R. Vajtai, A. D. Mohite and P. M. Ajayan, *ACS Nano*, 2014, **8**, 1263–1272.
34 Y. Ding and Y. Wang, *Appl. Phys. Lett.*, 2013, **103**, 043114.
35 E. Scalise, M. Houssa, E. Cinquanta, C. Grazianetti, B. van den Broek, G. Pourtois, A. Stesmans, M. Fanciulli and A. Molle, *2D Mater.*, 2014, **1**, 011010.
36 P. Giannozzi, S. Baroni, N. Bonini, M. Calandra, R. Car, C. Cavazzoni, D. Ceresoli, G. L. Chiarotti, M. Cococcioni, I. Dabo, A. Dal Corso, S. de Gironcoli, S. Fabris, G. Fratesi, R. Gebauer, U. Gerstmann, C. Gougoussis, A. Kokalj, M. Lazzeri, L. Martin-Samos, N. Marzari, F. Mauri, R. Mazzarello, S. Paolini, A. Pasquarello, L. Paulatto, C. Sbraccia, S. Scandolo, G. Sclauzero, A. P. Seitsonen, A. Smogunov, P. Umari and R. M. Wentzcovitch, *J. Phys.: Condens. Matter*, 2009, **21**, 395502.
37 G. Kresse and J. Furthmüller, *Phys. Rev. B: Condens. Matter Mater. Phys.*, 1996, **54**, 11169–11186.
38 M. Dion, H. Rydberg, E. Schröder, D. C. Langreth and B. I. Lundqvist, *Phys. Rev. Lett.*, 2004, **92**, 246401.
39 J. Klime, D. R. Bowler and A. Michaelides, *Phys. Rev. B: Condens. Matter Mater. Phys.*, 2011, **83**, 195131.
40 T. Thonhauser, V. R. Cooper, S. Li, A. Puzder, P. Hyldgaard and D. C. Langreth, *Phys. Rev. B: Condens. Matter Mater. Phys.*, 2007, **76**, 125112.
41 G. Román-Pérez and J. M. Soler, *Phys. Rev. Lett.*, 2009, **103**, 096102.
42 J. P. Perdew, K. Burke and M. Ernzerhof, *Phys. Rev. Lett.*, 1996, **77**, 3865.
43 H. J. Monkhorst and J. D. Pack, *Phys. Rev. B: Condens. Matter Mater. Phys.*, 1976, **13**, 5188–5192.
44 L. Bengtsson, *Phys. Rev. B: Condens. Matter Mater. Phys.*, 1999, **59**, 12301–12304.
45 G. Kresse and D. Joubert, *Phys. Rev. B: Condens. Matter Mater. Phys.*, 1999, **59**, 1758–1775.
46 J. Heyd, G. E. Scuseria and M. Ernzerhof, *J. Chem. Phys.*, 2003, **118**, 8207–8215.
47 J. Heyd, G. E. Scuseria and M. Ernzerhof, *J. Chem. Phys.*, 2006, **124**, 219906.
48 J. Heyd and G. E. Scuseria, *J. Chem. Phys.*, 2004, **121**, 1187–1192.
49 W. Tang, E. Sanville and G. Henkelman, *J. Phys.: Condens. Matter*, 2009, **21**, 084204.
50 G. Henkelman, A. Arnaldsson and H. Jónsson, *Comput. Mater. Sci.*, 2006, **36**, 354–360.
51 E. Sanville, S. D. Kenny, R. Smith and G. Henkelman, *J. Comput. Chem.*, 2007, **28**, 899–908.
52 F. Schwierz, *Nat. Nanotechnol.*, 2010, **5**, 487–496.
53 L. Matthes, O. Pulci and F. Bechstedt, *J. Phys.: Condens. Matter*, 2013, **25**, 395305.
54 G. Kresse, J. Furthmüller and J. Hafner, *Europhys. Lett.*, 2007, **32**, 729–734.
55 O. Dubay and G. Kresse, *Phys. Rev. B: Condens. Matter Mater. Phys.*, 2003, **67**, 035401.
56 J. Jiang, R. Saito, a. Grüneis, G. Dresselhaus and M. S. Dresselhaus, *Chem. Phys. Lett.*, 2004, **392**, 383–389.
57 M. W. Lin, C. Ling, L. A. Agapito, N. Kioussis, Y. Zhang, M. M.-C. Cheng, W. L. Wang, E. Kaxiras and Z. Zhou, *Phys. Rev. B: Condens. Matter Mater. Phys.*, 2011, **84**, 125411.
58 J. Wang, R. Zhao, M. Yang, Z. Liu and Z. Liu, *J. Chem. Phys.*, 2013, **138**, 084701.
59 Y. He and G. Galli, *Chem. Mater.*, 2014, **26**, 5394–5400.
60 A. Belsky, M. Hellenbrandt, V. L. Karen and P. Luksch, *Acta Crystallogr., Sect. B: Struct. Sci.*, 2002, **58**, 364–369.